Tantalum and Tantalum–Palladium Coated FBGs for Low-Concentration Hydrogen Sensing

Kasun Prabuddha Dissanayake, Ziqing Yuan, H. Sandra Dewi, Théo Travers, Herman Schreuders, Lars J. Bannenberg, and Roger M. Groves

***Abstract*—Hydrogen is a cornerstone of the emerging net-zero carbon economy, and its widespread deployment demands sensitive, stable, and scalable detection technologies. In this study, we present a comparative performance analysis of Fibre Bragg Grating (FBG) sensors coated with nanometre-thick metal hydride-forming layers—tantalum (Ta), tantalum-palladium alloy ($Ta_{0.88}Pd_{0.12}$), palladium (Pd), and palladium-gold alloy ($Pd_{0.6}Au_{0.4}$)—for optical hydrogen sensing. The integration of Ta and $Ta_{0.88}Pd_{0.12}$, two tantalum-based metal hydrides, with FBG sensors is introduced here for the first time, offering a promising alternative to conventional Pd-based materials. All coatings were deposited via magnetron sputtering and tested under controlled hydrogen exposure across concentrations ranging from 0.001% to 100% H_2. The Ta-based FBGs exhibited outstanding performance, showing a remarkably linear relative wavelength shift over the full tested range (0.001% to 100% H_2), with sensitivity detectable down to 10 ppm—the lowest concentration achievable in the current setup. Both Ta and $Ta_{0.88}Pd_{0.12}$ sensors exhibited fully reversible and hysteresis-free response characteristics, with rapid response and recovery. Among them, the $Ta_{0.88}Pd_{0.12}$ sensor with a 100 nm coating demonstrated the highest logarithmic sensitivity of ∼9 pm/decade(%H_2), corresponding to a 9 pm wavelength shift for every tenfold increase in hydrogen concentration between 0.001% and 100% H_2. In contrast, Pd and $Pd_{0.6}Au_{0.4}$ sensors showed degraded performance at low concentrations and greater signal hysteresis. These results underscore the potential of Ta and $Ta_{0.88}Pd_{0.12}$ coatings as robust and high-performance alternatives to conventional Pd-based materials for next-generation distributed fibre-optic hydrogen sensing systems.**

***Index Terms*—FBG, fibre optic sensors, hydrogen sensors, metal hydrides, palladium, tantalum.**

Received 31 July 2025; revised 17 September 2025; accepted 25 September 2025. Date of publication 1 October 2025; date of current version 6 April 2026. This work was supported in part by Clean Aviation Joint Undertaking and its members, through HYDEA project under Grant 101102019, and in part by Horizon Europe OVERLEAF project under Grant 101056818. *(Corresponding author: Kasun Prabuddha Dissanayake.)*

Kasun Prabuddha Dissanayake and H. Sandra Dewi are with the Department of Aerospace Structures, Materials, Faculty of Aerospace Engineering, Delft University of Technology, 2629 HS Delft, The Netherlands, and also with the Faculty of Applied Sciences, Delft University of Technology, 2629 HZ Delft, The Netherlands (e-mail: k.p.w.dissanayake@tudelft.nl).

Ziqing Yuan, Herman Schreuders, and Lars J. Bannenberg are with the Faculty of Applied Sciences, Delft University of Technology, 2629 HZ Delft, The Netherlands.

Théo Travers and Roger M. Groves are with the Department of Aerospace Structures, Materials, Faculty of Aerospace Engineering, Delft University of Technology, 2629 HS Delft, The Netherlands.

This article has supplementary material provided by the authors and color versions of one or more figures available at https://doi.org/10.1109/JLT.2025.3616783.

Digital Object Identifier 10.1109/JLT.2025.3616783

I. Introduction

As INDUSTRIES transition away from fossil fuels towards sustainable, carbon-free alternatives, hydrogen has emerged as a pivotal energy carrier in realising near-zero emission goals. Its high gravimetric energy density and clean combustion characteristics make it particularly attractive for applications ranging from energy storage and fuel cells to aviation and industrial processes [1], [2], [3]. However, hydrogen's low ignition energy and wide flammability range—starting at concentrations as low as 4% in air—necessitate the development of sensitive and reliable detection technologies to ensure operational safety [4].

Fibre optic sensors have shown considerable promise for hydrogen sensing due to their compact footprint, intrinsic safety (spark-free operation), immunity to electromagnetic interference, and suitability for remote or distributed sensing architectures [5]. Several fibre optic-based configurations have been reported, including grating based sensors [6], [7], [8], surface plasmon resonance sensors [9], Fabry–Pérot[10] and Mach–Zehnder [11] interferometers, and micro-mirror intensity sensors [12]. However, Fibre Bragg Gratings (FBGs) have gained increasing attention owing to their fabrication simplicity, ability for multipoint sensing via multiplexing, and capacity to deliver strain or temperature-modulated optical responses readily interrogated through wavelength shift measurements [13], [14], [15].

In hydrogen sensing applications, an FBG can be functionalised with a hydrogen-sensitive coating, typically a metal that absorbs hydrogen [16]. This absorption leads to volumetric expansion and stress in the coating, which induces a measurable axial strain on the underlying fibre. This strain shifts the Bragg wavelength proportionally, allowing the sensor to transduce hydrogen concentration into a robust optical signal. Palladium (Pd) has been the material of choice in many of these designs due to its high hydrogen solubility and excellent catalytic activity for hydrogen dissociation. Previous work includes Pd coated FBGs [13], [17] and also uncoated FBGs attached to Pd surfaces [18]. However, Pd suffers from drawbacks such as hysteresis—due to phase transitions at moderate concentrations, limited sensing range, and mechanical instability or delamination upon cyclic loading [19], [20]. These issues have prompted efforts to alloy Pd with elements such as gold (Au) to improve mechanical durability and suppress hysteresis [21], though this comes with a reduction in sensitivity due to lower hydrogen solubility and weaker response.

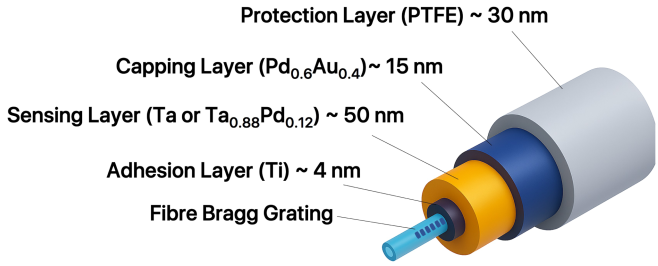

Fig. 1. Schematic of the FBG-based hydrogen sensor functionalised with tens of nanometre-thick metal hydride films of Ta and Ta $_{0.88}$ $Pd_{0.12}$, enabling sensitive and reversible H_2 detection. (Not to scale - Fibre diameter∼125 μm).

Tantalum (Ta) has recently emerged as a promising alternative due to its favourable hydride formation kinetics, high hydrogen solubility, minimal hysteresis, and mechanical robustness [6], [12], [22], [23], [24]. More importantly, Ta offers reliable sensing performance over a wide hydrogen concentration range and remains stable under ambient and elevated temperatures, making it well-suited for harsh environments [25]. In recent studies, alloying Ta with Pd has been proposed as a route to engineer the sensor response further by tuning the thermodynamics of hydrogen absorption, thereby improving sensitivity at both low and high hydrogen concentrations [24], [26].

This work presents the development of FBG-based hydrogen sensors coated with tens of nanometre-thick layers of Ta and $Ta_{0.88}Pd_{0.12}$, and compares their performance with Pd and $Pd_{0.6}Au_{0.4}$, aiming to highlight the unique hydrogen-sensing properties of Ta-based materials alongside the high sensitivity and multiplexing capabilities of FBGs. Building on preliminary findings presented at the Optical Fiber Sensors Conference (OFS-29) [27], it offers a comprehensive evaluation of sensor performance, including sensitivity, dynamics, and stability. While Pd-based coatings are well studied, the application of Ta and its Pd alloy to FBGs is, to the best of our knowledge, reported here for the first time. Sensors were tested from 0.001% to 100% H_2 in Ar, with emphasis on the low-concentration regime. The effect of film thickness was also examined by comparing 50 nm and 100 nm Ta$_{0.88}$ $Pd_{0.12}$ coatings. These Ta-based hydride-forming coatings are introduced here as promising alternatives for hydrogen sensing, offering improved performance in terms of sensitivity, reversibility, and detection at trace concentrations.

II. Hydrogen Sensing Thin Film Stack and Sensing Principle

A. Sensor Structure and Thin Film Stack Design

Each sensor comprises an FBG coated with a hydrogen-sensitive multilayer thin-film stack deposited onto the fibre cladding over the grating region. The coating induces hydrogen concentration-dependent optical responses primarily via strain transfer to the fibre core. A schematic illustration of the multilayer stack structure is shown in Fig. 1. The Ta and Ta $_{0.88}$ $Pd_{0.12}$ sensors feature a 4 nm Ti adhesion layer, a 50 nm sensing layer, a 15 nm Pd $_{0.6}$ $Au_{0.4}$ capping layer, and 30 nm PTFE overlayer. The Pd $_{0.6}$ $Au_{0.4}$ layer serves two purposes: it prevents oxidation of the underlying Ta-based film and facilitates hydrogen dissociation—a key step required for the hydrogen to be absorbed by the sensing material [16]. The Pd sensor uses a 4 nm Ti layer to promote adhesion, while the Pd $_{0.6}$ $Au_{0.4}$ sensor omits Ti since gold provides sufficient adhesion and Ti increases hysteresis in PdAu films [20]. All sensing layers are 50 nm thick, except for the second Ta $_{0.88}$ $Pd_{0.12}$ sensor, which was deliberately fabricated with a 100 nm sensing layer. A 30 nm PTFE overlayer is applied to all sensors to provide a chemically inert, hydrophobic barrier, enhancing selectivity against humidity and interfering gases (e.g., CO_2, NO_x) and supporting hydrogenation kinetics by preserving a clean catalytic interface and lowering the activation energy for hydrogen dissociation [28]. These configurations enable a systematic comparison of sensing performance across different metal compositions and film thicknesses.

B. Sensing Principle

The sensing principle is based on the absorption of hydrogen by the metallic layer (M + xH $\rightarrow$ MH_x). Upon exposure to hydrogen gas, molecular hydrogen dissociates catalytically on the metal surface and diffuses into the metal layer. This absorption causes volumetric expansion of the metal film, which induces axial strain $\varepsilon_{\text{metal}}$ in the multilayer stack. This strain is mechanically transferred to the fibre core, generating an axial strain ε_H on the FBG.

The FBG reflects light at a specific Bragg wavelength λ_B, defined as:

$$\lambda_B = 2n_{\text{eff}}\Lambda \tag{1}$$

where n_{eff} is the effective refractive index (RI) of the guided core mode and Λ is the grating period.

The ε_H alters both the Λ and the n_{eff} through the photoelastic effect, resulting in a shift in the Bragg wavelength.

This wavelength shift can be expressed as [29]:

$$\frac{\Delta\lambda_B}{\lambda_B} = (1 - P_e)\varepsilon_H = (1 - P_e)\,\alpha\,\varepsilon_{\text{metal}} \tag{2}$$

where P_e is the effective photo-elastic constant of the fibre, and α (where $0 < \alpha \leq 1$) represents the mechanical strain transfer efficiency from the metal coating to the fibre core.

Thus, the Bragg wavelength shift is directly proportional to the strain induced by the metal hydride expansion, enabling quantitative hydrogen sensing. This process is fully reversible, and the sensor's dynamic performance—including sensitivity, response/recovery times, and hysteresis—depends strongly on the thin-film material properties, thickness, and mechanical coupling to the fibre. In this context, the Ti adhesion layer plays a critical role by ensuring robust mechanical coupling between the fibre cladding and the functional film, thereby enhancing strain transfer efficiency and long-term film stability.

III. Sensor Fabrication

FBG hydrogen sensors were fabricated by depositing tens of nanometre-thick metal thin films (Ta, Ta $_{0.88}$ $Pd_{0.12}$, Pd, and Pd $_{0.6}$ $Au_{0.4}$) onto cleaned fibre surfaces via magnetron sputtering using an AJA International system. The fibres were cleaned with

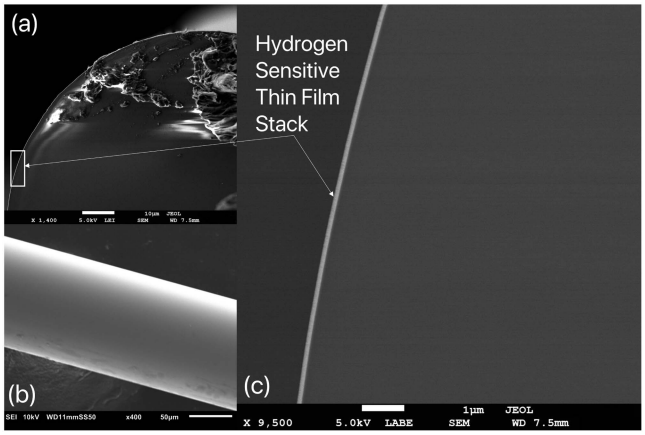

Fig. 2. SEM images of the Ta $_{0.88}$ Pd$_{0.12}$ 100 nm coated FBG sensor: (a) cross-sectional view of the fibre (LEI – Low-Energy Electron Mode), (b) side/surface view of the coated fibre (SEI – Secondary Electron Image Mode), and (c) zoomed cross-sectional image highlighting the nanometre-thick metal thin film stack on the fibre surface (LABE – Low Angle Backscattered Electron Mode).

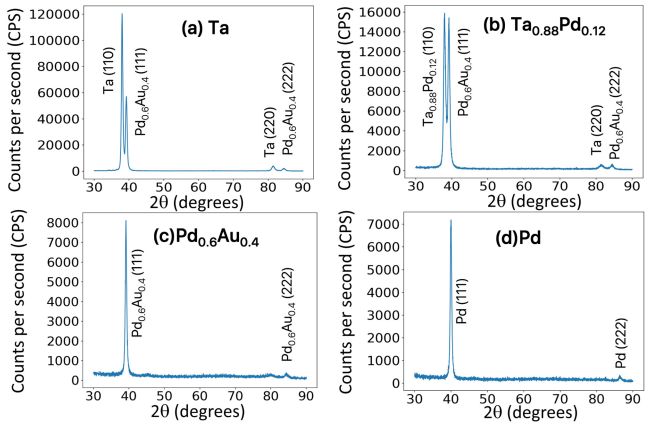

Fig. 3. X-ray diffraction (XRD) spectra of the four sensor coatings: (a) Ta, (b) Ta $_{0.88}$ Pd$_{0.12}$, (c) Pd $_{0.6}$ Au$_{0.4}$, and (c) Pd. Distinct peaks correspond to characteristic crystalline phases in each coating, confirming the successful deposition of well-defined metal thin film layers.

isopropyl alcohol prior to deposition to ensure optimal adhesion. Sputtering occurred in an argon (Ar) atmosphere at 0.3 Pa, with the fibre mounted on a rotating holder for uniform coating. The base pressure before deposition was 10^{-6} Pa. The sputtering parameters, including power, deposition rate, and time, were carefully controlled and are consistent with previously established protocols [23], [24], [25], allowing precise control over the film thicknesses. The Ta $_{0.88}$ Pd$_{0.12}$ and Pd $_{0.6}$ Au$_{0.4}$ alloy coatings were fabricated by co-sputtering from separate elemental targets simultaneously, with the sputtering powers adjusted to achieve the desired alloy compositions.

To enable detailed structural characterisation, a quartz substrate ($10 \times 10 \times 0.5$ mm) was placed adjacent to each FBG during deposition, ensuring that the same metal thin film stacks were formed simultaneously on both the substrate and the fibre surface. The quartz samples were subsequently analysed using X-ray diffraction (XRD) and X-ray reflectivity (XRR) via a Bruker D8 Discover X-Ray Diffractometer to determine the crystallographic phases and precise layer thicknesses.

Fig. 2 presents scanning electron microscope (SEM) images acquired using a JEOL JSM-7500F SEM, illustrating the coating uniformity of one of the Ta deposited fibres. Sub-figure (a) shows the cross-sectional view of the optical fibre, (b) depicts the fibre surface coated with the metal thin film, and (c) provides a zoomed image of the cross section, clearly resolving the nanometre-thick metal film stack.

Fig. 3 presents the XRD patterns of the four metal coatings deposited on quartz substrates. The Pd and $Pd_{0.6}Au_{0.4}$ layers exhibit characteristic diffraction peaks corresponding to the (111) and (222) planes of the Face-Centered Cubic (FCC) lattice, confirming their crystalline nature. The Ta and $Ta_{0.88}Pd_{0.12}$ coatings show the (110) and (220) reflections of the α-Ta phase - indicative of the Body-Centered Cubic (BCC) lattice structure. Although two $Ta_{0.88}Pd_{0.12}$ coatings of differing thicknesses were fabricated, only a representative XRD pattern is shown due to their similar structural signatures. These results confirm the successful deposition of the intended crystalline materials, with the fibre coatings expected to closely replicate those on the quartz reference substrates.

XRR measurements verified that the individual layer thicknesses closely matched the design specifications across all sensor variants, indicating high uniformity and reproducibility of the deposition process.

The FBGs used in this study were fabricated by B-Sens BV via phase mask inscription in standard photosensitive single-mode silica fibres without hydrogen loading. The fibre core and cladding refractive indices were 1.45 and 1.445, respectively, with a 125 μm cladding diameter. Each fibre segment was 50 mm in length, with a 10 mm-long FBG inscribed at its centre, and the sensing material stack was deposited over the entire 50 mm region. The five sensors employed Bragg wavelengths centred at 1524 nm, 1538 nm, or 1547 nm, with some sensors sharing the same Bragg wavelength. No polymer recoating was applied, leaving the cladding bare for direct thin-film deposition. All FBGs exhibited single-peak reflection spectra with FWHM between 0.15 nm and 0.2 nm, suitable for high-resolution interrogation of hydrogen-induced wavelength shifts.

IV. Experimental Configuration

The metal-coated FBG sensors were characterised in a leak-tight stainless steel chamber, allowing controlled exposure to varying hydrogen concentrations. Three gas cylinders—pure Ar, 4% H_2 in Ar, and 100% H_2—supplied the chamber via independently regulated Bronkhorst FlexiFlow Mass Flow Controllers (MFCs), enabling precise gas mixing and dilution. All experiments were conducted at room temperature (approximately 20 °C) and under atmospheric pressure within the gas cell. Before testing, sensors were stabilised under continuous Ar flow for two hours, followed by multiple full H_2 loading/purging cycles to eliminate initial stress artefacts and ensure repeatable responses. During measurements, total flow was maintained at 500 sccm.

Real-time H_2 concentrations were computed from second-by-second MFC data, allowing accurate step control across 17 levels

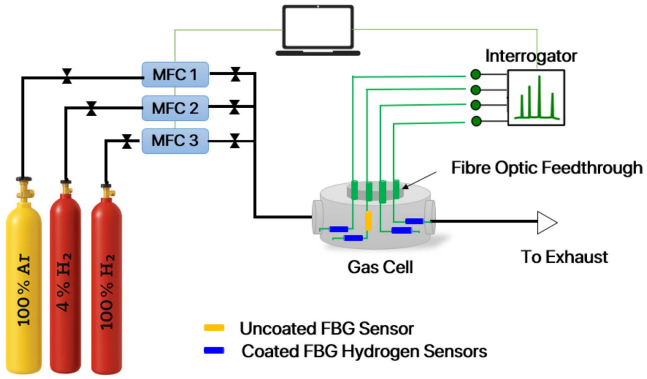

Fig. 4. Experimental setup for hydrogen sensing using metal-coated FBG sensors, including gas mixing via MFCs, a sealed gas chamber, and optical interrogation with the 4-Channel LUNA Hyperion Si155 system.

from 0.001% to 100% H_2 by volume (0.001%, 0.002%, 0.005%, 0.01%, 0.02%, 0.04%, 0.08%, 0.2%, 0.4%, 1%, 2%, 4%, 10%, 20%, 25%, and 100%). Sensors were mounted to ensure full exposure of the coated region without physical contact with chamber walls. An uncoated FBG positioned ∼20 mm from the coated gratings was used as a temperature and disturbance reference. By subtracting its response from that of the coated sensors, temperature-compensated hydrogen sensing signals were obtained.

Interrogation was performed using a LUNA Hyperion Si155 system (1 pm repeatability, 10 Hz sampling, 35 dB dynamic range). Fibres were routed through a hermetically sealed feedthrough (SQS Vláknová Optika A.S.), and Bragg wavelength data were averaged over a 100-point window to enhance stability and suppress noise. Each H_2 concentration step was held for 10 minutes to reach equilibrium. Full loading and purging cycles were repeated to evaluate sensitivity, reversibility, and hysteresis. The full setup is shown in Fig. 4.

V. Results and Discussion

A. Dynamic Hydrogen Response of the Metal Coated FBG Sensors

The hydrogen sensing performance of the metal-coated FBG sensors was evaluated across a full concentration cycle ranging from 0.001% to 100% and back to 0.001% H_2. The concentration was incrementally adjusted during both the absorption (loading) and desorption (unloading) phases to systematically assess sensitivity, reversibility, and hysteresis. Fig. 5(a) presents the time-dependent hydrogen concentration profile applied during the experiment. Fig. 5(b) displays the real-time Bragg wavelength shifts measured from the four FBG sensors coated with different hydrogen-sensitive materials. All sensors exhibit a characteristic red shift in Bragg wavelength with rising hydrogen concentration, followed by a corresponding decrease during desorption, driven by hydrogen-induced strain, ε_H in the sensing layers.

Several key trends can be observed. among the four coatings, Pure Pd exhibits the highest absolute shift, reaching approximately 22 pm at 100% H_2. However, it suffers from pronounced hysteresis between absorption and desorption phases, a consequence of hydrogen-induced phase transitions in the Pd lattice (well-known α–β phase transitions in Pd hydrides [13]). The addition of Au to form $Pd_{0.6}Au_{0.4}$ mitigates these phase transitions, resulting in reduced hysteresis. The incorporation of Au dampens the lattice expansion of Pd and suppresses abrupt structural transitions. However, this comes at the cost of reduced sensitivity, resulting in the smallest wavelength shift among the four coatings. These findings are in agreement with previously reported results on PdAu-based sensing materials [21]. Nonetheless, minor residual hysteresis is still evident in the $Pd_{0.6}Au_{0.4}$-coated sensor, likely due to plastic deformation in the 50 nm film upon some H_2 cycling. Moreover, the Pd-coated sensor displays noticeable baseline drift during certain hydrogen concentration steps—particularly at higher levels during loading and at lower levels during unloading—indicating instability and inconsistent equilibrium behaviour under static H_2 exposures. Additionally, both Pd and $Pd_{0.6}Au_{0.4}$-coated sensors show very low sensitivity at ppm-level hydrogen concentrations (below 0.1%), making them less suitable for low-concentration detection applications.

In contrast, the Ta and $Ta_{0.88}Pd_{0.12}$ coatings show remarkable reversibility, negligible hysteresis, and a clearly distinguishable step response even at hydrogen concentrations as low as 0.001%. The absence of hysteresis is attributed to the fact that these materials do not undergo hydride phase transitions within the tested concentration range. This behaviour is consistent with the suppression of phase transformations, elastic lattice expansion, and the formation of a solid solution throughout the entire range of hydrogen concentrations studied [22], [23]. Both coatings exhibit an immediate ∼3 pm shift when transitioning from the baseline to 0.001% H_2, suggesting strong potential for detecting even lower hydrogen concentrations—currently limited by the achievable minimum concentration in the experimental setup. Notably, the $Ta_{0.88}Pd_{0.12}$ sensor achieves a peak shift of nearly 20 pm, approaching that of pure Pd but without any significant hysteresis, highlighting its excellent sensing performance and full reversibility.

B. Logarithmic Response Behaviour Across the Full Hydrogen Concentration Range

To more clearly visualise the response behaviour, Fig. 5(c) plots the steady-state wavelength shift as a function of hydrogen concentration on a logarithmic x-axis. For each material, distinct loading (solid lines) and unloading (dashed lines) curves are shown, enabling direct assessment of hysteresis. This representation highlights the full dynamic range of the sensors, spanning five orders of magnitude in H_2 concentration. All four sensors—Pd, $Pd_{0.6}Au_{0.4}$, Ta, and $Ta_{0.88}Pd_{0.12}$—exhibit monotonic increases in Bragg wavelength with increasing hydrogen concentration. However, the rate and extent of these shifts vary considerably between coatings. The Ta- and $Ta_{0.88}Pd_{0.12}$-coated sensors exhibit a quasi-linear dependence of the wavelength shift on the logarithm of the hydrogen concentration for H_2 levels above 0.01%. Among the coatings showing minimal hysteresis, the $Ta_{0.88}Pd_{0.12}$ sensor displays the steepest slope, indicating the highest sensitivity across the entire hydrogen concentration

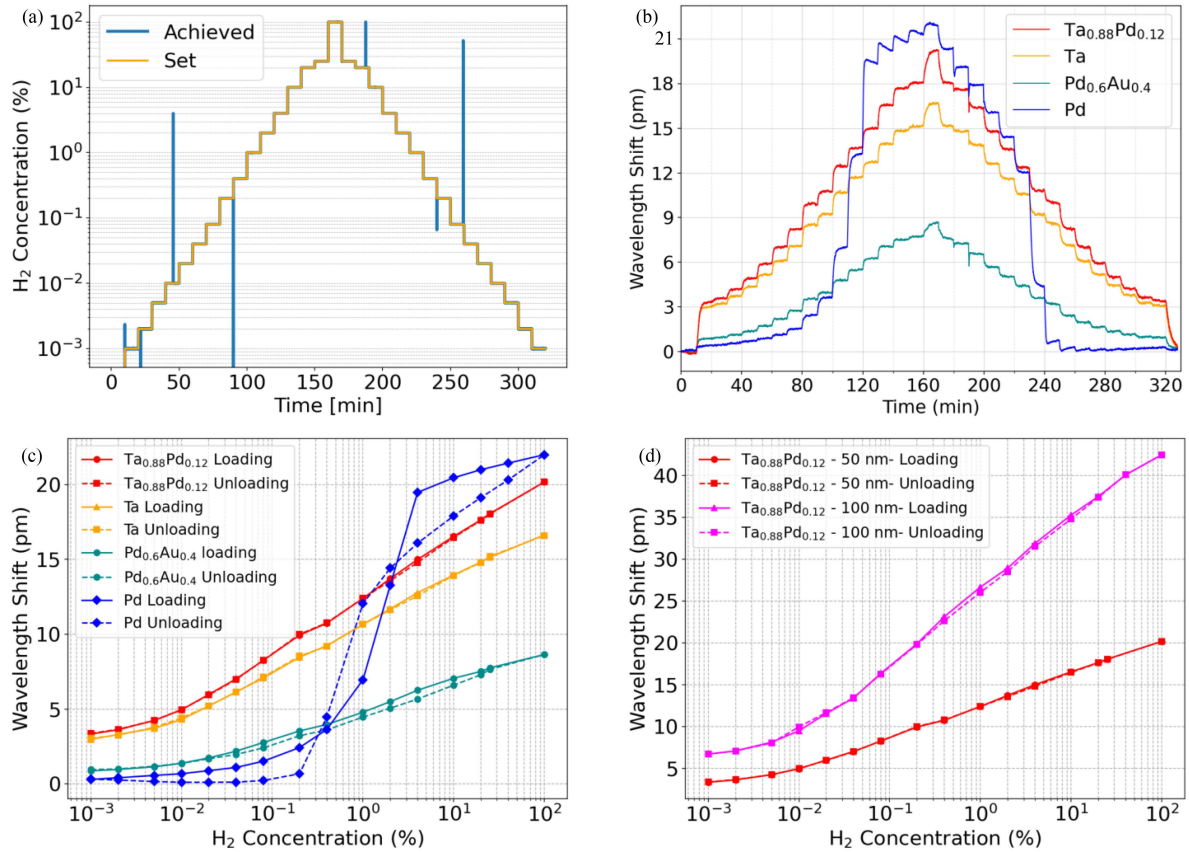

Fig. 5. Hydrogen sensing performance of FBGs coated with Ta, Ta $_{0.88}$ Pd$_{0.12}$, Pd $_{0.6}$ Au$_{0.4}$, and Pd. (a) Time-dependent hydrogen concentration profile applied during the experiment. (b) Real-time Bragg wavelength shifts measured from the four coated FBG sensors (50 nm sensing layer), showing distinct responses depending on the sensing material. (c) Steady-state wavelength shift as a function of hydrogen concentration on a logarithmic scale, highlighting the improved sensitivity of Ta and Ta $_{0.88}$ Pd$_{0.12}$ sensors at low concentrations. (d) Comparison of the wavelength response of Ta $_{0.88}$ Pd$_{0.12}$-coated FBGs with 50nm and 100nm film thicknesses, demonstrating enhanced performance with increased coating thickness.

range. The pure Ta-coated sensor follows closely, also demonstrating a consistent logarithmic response extending from the low ppm regime up to 100% H_2. This behaviour is particularly advantageous for the detection of low hydrogen concentrations, enhancing the suitability of these sensors for safety-critical applications.

Compared to the Pd-alloy ($Pd_{0.6}Au_{0.4}$), the enhanced hydrogen sensitivity of Ta-based materials at low concentrations can be attributed to their ability to detect hydrogen over a broader pressure range—spanning up to seven orders of magnitude at room temperature-compared to four orders for PdAu [22]. Furthermore, the higher sensitivity of $Ta_{0.88}Pd_{0.12}$ relative to pure Ta likely arises from its greater lattice expansion within the tested concentration window, resulting in increased in-plane strain and a larger Bragg wavelength shift [22].

Fig. 5(d) compares the hydrogen sensing responses of FBG sensors coated with 50 nm and 100 nm $Ta_{0.88}Pd_{0.12}$ layers, presented as wavelength shift versus hydrogen concentration on a logarithmic scale. $Ta_{0.88}Pd_{0.12}$ was chosen for this thickness-dependent analysis due to its superior sensitivity observed in the 50 nm comparison. Both thicknesses exhibit comparable logarithmic responses across the entire concentration range, demonstrating good reproducibility and robustness of the sensing behaviour.

However, the sensor with the 100 nm coating consistently shows more than double the wavelength shift at each concentration step compared to the 50 nm variant. This clear enhancement in signal magnitude indicates that increasing the coating thickness substantially improves the sensitivity of the sensor. Despite this improvement, the 100 nm thickness remains relatively modest when compared to those reported in literature for FBG hydrogen sensors [13], [17], suggesting further optimisation potential for boosting performance through controlled thickness tuning.

To quantify, the 100 nm $Ta_{0.88}Pd_{0.12}$ coating exhibits the highest sensitivity, reaching approximately 9pm/decade(%H_2). This is more than double the response of the 50 nm $Ta_{0.88}Pd_{0.12}$ coating, which shows a sensitivity of around 4 pm/decade(%H_2). Pure Ta follows closely with a sensitivity of approximately 3.5 pm/decade(%H_2). These sensitivities for Ta-based coatings are significantly higher than those of the Pd and $Pd_{0.6}Au_{0.4}$ sensors below 2% H_2 (low) concentration range.

C. Stability and Repeatability Under Cyclic Hydrogen Exposure

Fig. 6 presents the cyclic hydrogen response of the five coated FBG sensors subjected to alternating exposures of 0.1% and 4%

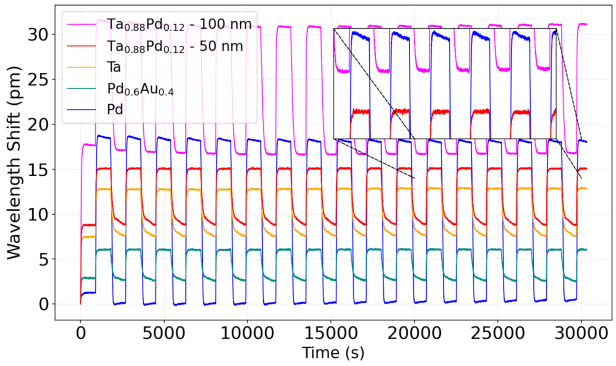

Fig. 6. Cycling stability of coated FBG sensors between 0.1% and 4% H_2. The inset shows baseline drift in Pd versus stable response in $Ta_{0.88}Pd_{0.12}$.

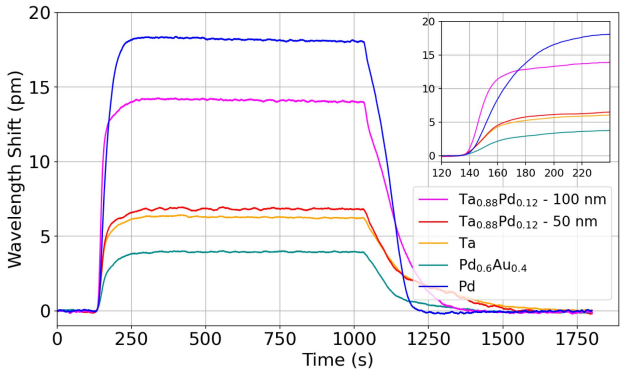

Fig. 7. Response time (t_{90}) of the FBG sensors for a step change from 0.1% to 4% hydrogen concentration.

H_2, with each step lasting 15 minutes. The Ta-based sensors, including both pure Ta and $Ta_{0.88}Pd_{0.12}$ alloys, exhibit sharp, step-like, and highly repeatable spectral responses across all cycles. These abrupt and nearly symmetric transitions reflect rapid and reversible hydrogen absorption and desorption within the Ta-based metal hydride layers, underscoring their fast reaction kinetics and excellent reproducibility. With little to no signal degradation or hysteresis observed across cycles, the amplitude of the response remains stable and the baseline shows negligible drift, confirming the robustness of these coatings under dynamic hydrogen conditions.

The $Pd_{0.6}Au_{0.4}$ sensor also performs well, demonstrating consistent cycling behaviour and signal stability. However, the Pd-coated sensor shows noticeable baseline drift at both 0.1% and 4% H_2, indicating poorer reversibility and potential instability of pure Pd under repeated hydrogenation–dehydrogenation. This underscores the improved stability achieved through Pd alloying and the superior long-term robustness of Ta-based coatings compared to pure Pd.

D. Response Time Analysis

To assess the dynamic response characteristics of the sensors, a representative hydrogenation step—from 0.1% to 4.0% H_2—was extracted from the previously presented stability measurements (Fig. 6) and analysed in detail. The time-resolved wavelength shift data were normalised to facilitate a direct comparison of the response dynamics across different coatings. Fig. 7 presents a comparative overview of the wavelength shifts following the hydrogen step. The response time was defined as the time to reach 90% of the final shift, extracted from the rising edge shown in the zoomed-in inset.

Among all configurations, the 100 nm $Ta_{0.88}Pd_{0.12}$ coating exhibited the fastest response, reaching 90% of the final Bragg wavelength shift in just 46 s. These Ta-based sensors consistently demonstrated faster response times—70s for the 50 nm $Ta_{0.88}Pd_{0.12}$ and 71 s for pure Ta—compared to Pd-based coatings. For instance, the $Pd_{0.6}Au_{0.4}$ sensor required 84 s. This rapid behaviour is attributed to the intrinsically high hydrogen diffusivity of Ta, which exceeds that of Pd by several orders of magnitude at room temperature. The open BCC crystal structure of Ta provides less steric hindrance to hydrogen atoms, allowing for faster absorption and diffusion through the film [30]. This makes Ta and its alloys particularly advantageous for applications requiring fast hydrogen sensing. The faster response observed in the $Ta_{0.88}Pd_{0.12}$-coated sensor compared to the pure Ta-coated sensor can also be attributed to the structural effect of Pd alloying. The incorporation of Pd into the Ta lattice reduces the unit cell volume, thereby decreasing the number of hydrogen atoms required to reach a given equilibrium concentration. As a result, the system attains a stable hydride state more rapidly, leading to a shorter response time under identical hydrogen exposure conditions. Interestingly, the thicker 100 nm $Ta_{0.88}Pd_{0.12}$ coating outperformed its thinner 50 nm counterpart. Although thicker films typically exhibit slower response times due to longer diffusion paths, this counter-intuitive trend may be attributed to improved film quality, enhanced microstructural uniformity, or reduced surface contamination in the thicker alloy layers. Variations in the PTFE passivation layer morphology or porosity, which influences hydrogen permeability, may also contribute to these differences.

It should be emphasised that these response times are influenced by both intrinsic material kinetics and extrinsic factors. All sensors were characterised in a 0.4 L gas cell, where hydrogen flow rates affect the time required for sensor surface saturation. Therefore, the measured response times represent a convolution of intrinsic absorption and diffusion kinetics with external gas transport dynamics. Nevertheless, intrinsic studies on Ta and $Ta_{0.88}Pd_{0.12}$ materials have demonstrated sub-second hydrogen response times [22], [26], highlighting their strong potential for rapid and reversible hydrogen sensing when extrinsic limitations are minimised.

VI. Conclusion

We demonstrated the hydrogen sensing performance of FBGs coated with nanometre-scale metal hydride thin films, including Ta, TaPd alloy ($Ta_{0.88}Pd_{0.12}$), Pd, and a PdAu alloy ($Pd_{0.6}Au_{0.4}$). The sensors were tested across five orders of magnitude in hydrogen concentration, from 0.001% H_2 to 100% H_2, revealing distinct trends in both absolute response and cycling behaviour. The aim of this study was to assess the impact of coating composition and thickness on key sensor performance indicators, including sensitivity, response time, and stability.

The Ta-coated FBG exhibited excellent stability, reproducibility, and a linear Bragg wavelength shift with respect to the

logarithm of hydrogen concentration. Remarkably, it maintained nearly constant relative sensitivity across the entire tested range, with little to no signal degradation or hysteresis observed across repeated cycles. Similarly, both the 50 nm and 100 nm Ta $_{0.88}$ $Pd_{0.12}$-coated sensors exhibited highly stable and reversible responses. The 100 nm Ta $_{0.88}$ $Pd_{0.12}$ sensor, in particular, demonstrated the largest absolute wavelength shift of 42 pm at 100% H_2, outperforming all other sensors in terms of signal strength, while retaining excellent cycling and response time characteristics. It showed a sensitivity of ∼9 pm/decade(%H_2) and a response time of approximately 46s for a step change from 0.1% to 4% H_2. All Ta-based sensors were able to detect concentrations as low as 10 ppm, with this lower limit set by the capabilities of the experimental setup.

In contrast, the Pd and Pd $_{0.6}$ $Au_{0.4}$-coated FBGs displayed significant hysteresis and very low sensitivity at ppm levels. The Pd sensor, although yielding high wavelength shifts at elevated hydrogen concentrations, suffered from pronounced instability during stepped cycling between 0.1–4% H $_2$. The $Pd_{0.6}$ $Au_{0.4}$ sensor displayed improved reversibility compared to Pd, but still suffered from noticeable hysteresis and lower sensitivity.

Overall, this study demonstrates that Ta and TaPd-coated FBG sensors offer a compelling combination of high sensitivity, fast response, and stable, reproducible performance—outperforming conventional Pd and PdAu-coated alternatives in nearly all key sensing metrics. These findings highlight the potential of Ta-based metal hydride coatings as a robust platform for fibre-optic hydrogen sensing, especially in distributed monitoring applications where long-term stability, wide dynamic range, and low detection limits are critical. Future work will focus on optimizing film thickness to enhance both sensitivity and response time, as well as exploring alternative alloy compositions such as tantalum-ruthinium [23] to further improve sensor performance and durability.

ACKNOWLEDGMENT

The materials used are covered under patent EP 4 241 070 A1, owned by Delft University of Technology, with inventors Lars Johannes Bannenberg and Herman Schreuders.

REFERENCES

[1] J. Eissele et al., "Hydrogen-powered aviation—Design of a hybrid-electric regional aircraft for entry into service in 2040," *Aerospace*, vol. 10, no. 3, 2023, Art. no. 277.

[2] M. A. Sattar, M. G. Rasul, M. I. Jahirul, and M. M. Hasan, "An up-to-date review on the progress and challenges of hydrogen storage, and its safety and economic analysis," *Sustain. Energy Fuels*, vol. 8, pp. 3545–3573, 2024.

[3] I. Staffell et al., "The role of hydrogen and fuel cells in the global energy system," *Energy Environ. Sci.*, vol. 12, no. 2, pp. 463–491, 2019.

[4] U. S. Department of Energy, "Hydrogen safety," (n.d.). Accessed: Jul. 28, 2025. [Online]. Available: https://www1.eere.energy.gov/hydrogenandfuelcells/pdfs/h2_safety_fsheet.pdf

[5] Y. nan Zhang, H. Peng, X. Qian, Y. Zhang, G. An, and Y. Zhao, "Recent advancements in optical fiber hydrogen sensors," *Sensors Actuators B, Chem.*, vol. 244, pp. 393–416, 2017.

[6] K. Dissanayake, H. Dewi, H. Schreuders, L. Bannenberg, and R. Groves, "Advancing hydrogen sensing for sustainable aviation: A metal hydride coated TFBG optical fibre hydrogen sensor," in *Proc. 10th Eur. Workshop Struct. Health Monit.*, Potsdam, Germany, Jun. 2024.

[7] J. Yu, Z. Wu, X. Yang, X. Han, and M. Zhao, "Tilted fiber Bragg grating sensor using chemical plating of a palladium membrane for the detection of hydrogen leakage," *Sensors*, vol. 18, no. 12, 2018, Art. no. 4478.

[8] F. Zhang et al., "Optical fiber hydrogen sensor based on π-phase-shifted grating and sputtered Pd/Hf composite film," *Photonic Sensors*, vol. 15, 2025, Art. no. 250204.

[9] A. Hosoki, M. Nishiyama, H. Igawa, A. Seki, and K. Watanabe, "A hydrogen curing effect on surface Plasmon resonance fiber optic hydrogen sensors using an annealed Au/Ta_2O_5/Pd multilayer film," *Opt. Exp.*, vol. 22, pp. 18556–18563, 2014.

[10] B. Du et al., "Highly sensitive hydrogen sensor based on an in-fiber Mach-Zehnder interferometer with polymer infiltration and PT-loaded WO_3 coating," *Opt. Exp.*, vol. 29, no. 3, pp. 4147–4158, Feb. 2021.

[11] J. Luo et al., "Fiber optic hydrogen sensor based on a Fabry–Perot interferometer with a fiber Bragg grating and a nanofilm," *Lab Chip*, vol. 21, pp. 1752–1758, 2021.

[12] D. Verhoeff, H. Schreuders, and L. Bannenberg, "Tantalum-palladium alloy based optical micro-mirror hydrogen sensor," *Sensors Actuators B, Chem.*, vol. 428, 2025, Art. no. 137229.

[13] Y. Chen, Y. Yang, C. Liang, Y. Yao, and J. Chen, "Palladium-based optical fiber Bragg grating hydrogen sensors: A comprehensive review," *Opt. Laser Technol.*, vol. 175, 2024, Art. no. 110850.

[14] X. Ping et al., "Fiber grating hydrogen sensor: Progress, challenge and prospect," *Adv. Sensor Res.*, vol. 3, no. 2, 2024, Art. no. 2300088.

[15] X. Zhou, Y. Dai, J. M. Karanja, F. Liu, and M. Yang, "Microstructured FBG hydrogen sensor based on PT-loaded WO_3," *Opt. Exp.*, vol. 25, no. 8, pp. 8777–8786, Apr. 2017.

[16] L. J. Bannenberg, C. Boelsma, K. Asano, H. Schreuders, and B. Dam, "Metal hydride based optical hydrogen sensors," *J. Phys. Soc. Jpn.*, vol. 89, no. 5, 2020, Art. no. 051003.

[17] S. Saad and L. Hassine, "Hydrogen detection with FBG sensor technology for disaster prevention," *Photonic Sensors*, vol. 3, pp. 214–223, 2013.

[18] M. Fisser, R. A. Badcock, P. D. Teal, and A. Hunze, "High-sensitivity fiber-optic sensor for hydrogen detection in gas and transformer oil," *IEEE Sensors J.*, vol. 19, no. 9, pp. 3348–3357, May 2019.

[19] "Boosting room temperature response of Pd-based hydrogen sensor by constructing in situ nanoparticles," *Physica E, Low-Dimensional Syst. Nanostructures*, vol. 144, 2022, Art. no. 115464.

[20] B. Toksha, P. Gupta, and M. Rahaman, "Hydrogen sensing with palladium-based materials: Mechanisms, challenges, and opportunities," *Chem.– Asian J.*, vol. 19, no. 16, 2024, Art. no. e202400127.

[21] L. J. Bannenberg et al., "Direct comparison of PdAu alloy thin films and nanoparticles upon hydrogen exposure," *ACS Appl. Mater. Interfaces*, vol. 11, no. 17, pp. 15489–15497, 2019.

[22] L. Bannenberg, H. Schreuders, and B. Dam, "Tantalum-palladium: Hysteresis-free optical hydrogen sensor over 7 orders of magnitude in pressure with sub-second response," *Adv. Funct. Mater.*, vol. 31, no. 16, 2021, Art. no. 2010483.

[23] L. J. Bannenberg et al., "Tuning the properties of thin-film TaRu for hydrogen-sensing applications," *ACS Appl. Mater. Interfaces*, vol. 15, no. 6, pp. 8033–8045, 2023.

[24] L. J. Bannenberg, D. J. Verhoeff, N. Jonckers Newton, M. Thijs, and H. Schreuders, "Structural and optical properties of thin film β-Ta upon exposure to hydrogen to assess its applicability as hydrogen sensing material," *ACS Appl. Nano Mater.*, vol. 7, no. 2, pp. 1757–1766, 2024.

[25] H. Dewi, K. Dissanayake, H. Schreuders, R. Groves, and L. Bannenberg, "Metal hydride hydrogen sensing materials from 28 °C to 270 °C," *Int. J. Hydrogen Energy*, vol. 84, pp. 606–614, 2024.

[26] Z. Yuan, H. Schreuders, R. Dankelman, B. Dam, and L. J. Bannenberg, "Optical hydrogen sensing materials for applications at sub-zero temperatures," *Adv. Funct. Mater.*, vol. 35, 2025, Art. no. 2420087.

[27] K. P. Dissanayake, H. S. Dewi, Z. Yuan, H. Schreuders, L. J. Bannenberg, and R. M. Groves, "A step towards multipoint hydrogen sensing: Development of metal hydride-coated FBG hydrogen sensors," *Proc.SPIE*, vol. 13639, 2025, Art. no. 136399A.

[28] L. J. Bannenberg, B. Boshuizen, F. A. A. Nugroho, and H. Schreuders, "Hydrogenation kinetics of metal hydride catalytic layers," *ACS Appl. Mater. Interfaces*, vol. 13, pp. 52530–52541, 2021.

[29] M. Majumder, T. K. Gangopadhyay, A. K. Chakraborty, K. Dasgupta, and D. Bhattacharya, "Fibre Bragg gratings in structural health monitoring—Present status and applications," *Sensors Actuators A, Phys.*, vol. 147, no. 1, pp. 150–164, 2008.

[30] Y. Fukai, "The metal-hydrogen system: Basic bulk properties," *Springer Berlin Heidelberg*, pp. 303–400, 2005, doi: 10.1007/3-540-28883-X_6.